8558 *Inorg. Chem.* **2010**, *49*, 8558–8567
DOI: 10.1021/ic101178n

Inorganic Chemistry
Article

Interaction of Cationic Nickel and Manganese Porphyrins with the Minor Groove of DNA

Carmen Romera, Laurent Sabater, Antonio Garofalo, Isabelle M. Dixon, and Geneviève Pratviel*

CNRS, Laboratoire de Chimie de Coordination, 205 route de Narbonne, F-31077 Toulouse, France, Université de Toulouse, F-31077 Toulouse, France

Received June 11, 2010

The capacity of a series of new cationic nickel and manganese metalloporphyrins to bind in the minor groove of DNA was evaluated by binding competition experiments with manganese(III)-bis-aqua-*meso*-tetrakis(4-*N*-methylpyridiniumyl)-porphyrin, Mn-TMPyP, a powerful artificial nuclease when associated with $KHSO_5$. The four *N*-methylpyridiniumyl substituents on this porphyrin macrocycle are responsible for a strong binding affinity for the minor groove of AT-rich DNA. The inhibition of DNA cleavage mediated by Mn-TMPyP/$KHSO_5$ by the various tested porphyrins correlated with their competitive occupancy of the minor groove site of Mn-TMPyP. Introduction of long and flexible cationic substituents at the periphery of the porphyrin macrocycle precluded the interaction of the porphyrin derivative in the minor groove and resulted in low affinity for DNA. On the other hand, introduction of phenylpyridiniumyl substituents on the porphyrin macrocycle surprisingly conferred the new porphyrin derivative with a tight binding in the minor groove of a six consecutive AT base pairs sequence. These data on structural requirements for minor groove DNA binding will help the rational design of porphyrin derivatives for selective targeting of quadruplex DNA versus double-stranded DNA.

Introduction

Because of their large aromatic core able to undergo $\pi-\pi$ stacking interactions with guanine quartets of quadruplex DNA, porphyrins have appeared as promising quadruplex DNA ligands[1−16] and have been tested as anticancer agents.[5,17−22] The non-metalated derivative of *meso*-tetrakis(4-*N*-methylpyridiniumyl)porphyrin (H_2-TMPyP) became a standard G4-ligand.[1] However, H_2-TMPyP is not a selective quadruplex DNA ligand. The large aromatic core of the porphyrin is also compatible with intercalation between the base pairs of DNA, which confers a high affinity binding constant for double-stranded DNA ($K_A \approx 10^6\ M^{-1}$).[23−25] Insertion of a metal ion bearing axial ligands in the center of the porphyrin prevents intercalation[23−25] as well as the addition of bulky substituents at the *meso* positions of the porphyrin macrocycle.[26] On the other hand, neither bulky substituents at the periphery

*To whom correspondence should be addressed. E-mail: genevieve.pratviel@lcc-toulouse.fr.

(1) Wheelhouse, R. T.; Sun, D.; Han, H.; Xiaoguang Han, F.; Hurley, L. H. *J. Am. Chem. Soc.* **1998**, *120*, 3261–3262.
(2) Vialas, C.; Pratviel, G.; Meunier, B. *Biochemistry* **2000**, *39*, 9514–9522.
(3) Han, H.; Langley, D. R.; Rangan, A.; Hurley, L. H. *J. Am. Chem. Soc.* **2001**, *123*, 8902–8913.
(4) Siddiqui-Jain, A.; Grand, C. L.; Bearss, D. J.; Hurley, L. H. *Proc. Natl. Acad. Sci. U.S.A.* **2002**, *99*, 11593–11598.
(5) Lemarteleur, T.; Gomez, D.; Paterski, R.; Mandine, E.; Mailliet, P.; Riou, J.-F. *Biochem. Biophys. Res. Commun.* **2004**, *323*, 802–808.
(6) Phan, A. T.; Kuryavyi, V.; Gaw, H. Y.; Patel, D. J. *Nat. Chem. Biol.* **2005**, *1*, 167–173.
(7) Dixon, I. M.; Lopez, F.; Esteve, J. P.; Tejera, A. M.; Blasco, M. A.; Pratviel, G.; Meunier, B. *ChemBioChem* **2005**, *6*, 123–132.
(8) Yamashita, T.; Uno, T.; Ishikawa, Y. *Bioorg. Med. Chem.* **2005**, *13*, 2423–2430.
(9) Cogoi, S.; Xodo, L. E. *Nucleic Acids Res.* **2006**, *34*, 2536–2549.
(10) Parkinson, G. N.; Ghosh, R.; Neidle, S. *Biochemistry* **2007**, *46*, 2390–2397.
(11) Dixon, I. M.; Lopez, F.; Tejera, A. M.; Esteve, J. P.; Blasco, M. A.; Pratviel, G.; Meunier, B. *J. Am. Chem. Soc.* **2007**, *129*, 1502–1503.
(12) Evans, S. E.; Mendez, M. A.; Turner, K. B.; Keating, L. R.; Grimes, R. T.; Melchoir, S.; Szalai, V. A. *J. Biol. Inorg. Chem.* **2007**, *12*, 1235–1249.
(13) Wei, C.; Jia, G.; Zhou, J.; Han, G.; Li, C. *Phys. Chem. Chem. Phys.* **2009**, *11*, 4025–4032.
(14) McGuire, R., Jr.; McMillin, D. R. *Chem. Commun.* **2009**, 7393–7395.
(15) del Toro, M.; Bucek, P.; Avino, A.; Jaumot, J.; Gonzalez, C.; Eritja, R.; Gargallo, R. *Biochimie* **2009**, *91*, 894–902.
(16) Du, Y.; Zhang, D.; Chen, W.; Zhang, M.; Zhou, Y.; Zhou, X. *Bioorg. Med. Chem.* **2010**, *18*, 1111–1116.
(17) Izbicka, E.; Nishioka, D.; Marcell, V.; Raymond, E.; Davidson, K. K.; Lawrence, R. A.; Wheelhouse, R. T.; Hurley, L. H.; Wu, R. S.; Von Hoff, D. D. *Anti-Cancer Drug Des.* **1999**, *14*, 355–365.
(18) Shi, D. F.; Wheelhouse, R. T.; Sun, D.; Hurley, L. H. *J. Med. Chem.* **2001**, *44*, 4509–4523.
(19) Grand, C. L.; Han, H.; Munoz, R. M.; Weitman, S.; Von Hoff, D. D.; Hurley, L. H.; Bearss, D. J. *Mol. Cancer Ther.* **2002**, *1*, 565–573.
(20) Kim, M. Y.; Gleason-Guzman, M.; Izbicka, E.; Nishioka, D.; Hurley, L. H. *Cancer Res.* **2003**, *63*, 3247–3256.
(21) Mikami-Terao, Y.; Akiyama, M.; Yuza, Y.; Yanagisawa, T.; Yamada, O.; Yamada, H. *Cancer Lett.* **2008**, *261*, 226–234.
(22) Haeubl, M.; Schuerz, S.; Svejda, B.; Reith, L. M.; Gruber, B.; Pfragner, R.; Schoefberger, W. *Eur. J. Med. Chem.* **2010**, *45*, 760–773.
(23) Kelly, J. M.; Murphy, M. J.; McConnell, D. J.; OhUigin, C. *Nucleic Acids Res.* **1985**, *13*, 167–184.
(24) Fiel, R. J. *J. Biomol. Struct. Dyn.* **1989**, *6*, 1259–1274.
(25) Geacintov, N. E.; Ibanez, V.; Rougee, M.; Bensasson, R. V. *Biochemistry* **1987**, *26*, 3087–3092.
(26) Ford, K. G.; Neidle, S. *Bioorg. Med. Chem.* **1995**, *3*, 671–677.

Published on Web 08/17/2010

of the porphyrin[11,13,27] nor axial ligands on the central metal[7,11] preclude the binding of a porphyrin to quadruplex DNA. Consequently, it seems relatively easy to design porphyrin derivatives that interact with quadruplex DNA but do not interact with double-stranded DNA through the intercalation binding mode. Unfortunately, intercalation is not the only mode of binding of cationic porphyrins with DNA. Interaction in the minor groove is also a tight binding process for H_2-TMPyP and its metalated derivatives.[23−25] Thus, a better understanding of the general rules for porphyrin−DNA interaction in the minor groove is necessary for the design of quadruplex selective porphyrin-based compounds.

A number of positively charged compounds are capable of specific recognition of DNA through the minor groove of AT-rich sequences. This interaction is due to a special negative potential of regions rich in AT pairs.[28,29] The proper fitting of the dye with the minor groove is most of the time associated with a strong interaction.[30] The shape of the molecule may complement the bend of the DNA double helix. Spermine,[31] distamycin A,[32] netropsin,[33] Hoechst 33258,[34] and pyrrole-imidazole polyamides[35−37] are typical examples. They are crescent shaped and positively charged molecules. Additionally, they afford several suitable hydrogen bondings inside the minor groove.[38−40]

However, hydrogen bondings are not required for a drug to undergo strong binding in the minor groove.[41] The manganese derivative of H_2-TMPyP, manganese(III)-bis-aqua-*meso*-tetrakis(4-*N*-methylpyridiniumyl)porphyrin, Mn-TMPyP, is able to bind in the minor groove of AT-rich sequences of DNA with an affinity binding constant on the order of 10^6-10^7 M^{-1}.[23,42−47] The minor groove location of this porphyrin was unambiguously established by the 3′-shifted oxidative cleavage of DNA mediated by Mn-TMPyP porphyrin when activated into an artificial nuclease by addition of $KHSO_5$.[44,47] In the absence of structural data of the porphyrin/DNA complex, modeling studies provide a depiction of the interaction.[45] The porphyrin framework of Mn-TMPyP is devoid of any H-bonding donor/acceptor capacity. The porphyrin DNA binding is probably electrostatic in nature due to the positive charges at the *N*-methylpyridiniumyl groups yet associated with a special spatial fitting between the porphyrin and the curved DNA.

Using different cationic nickel and manganese porphyrin derivatives, we explored the structural requirements for a porphyrin to bind in the minor groove of DNA. The first tested porphyrins were nickel porphyrins that are redox inactive and consequently are unable to cleave DNA. The ability of the new nickel porphyrins to interact in the minor groove of AT-rich sequences was evaluated by the measurement of their inhibition of the Mn-TMPyP/$KHSO_5$ nuclease activity by competitive residence in the DNA minor groove. Further insight into the location of the porphyrin ligands with respect to DNA was gained by investigating their potency as new artificial nucleases in the presence of $KHSO_5$, when they were metalated with manganese. Introduction of long and flexible cationic substituents at the four *meso*-positions of the porphyrin macrocycle precluded the interaction of the porphyrin in the minor groove and resulted in an overall low affinity for DNA. On the other hand, extending the hydrophobic character of the porphyrin by replacing pyridiniumyl by phenylpyridiniumyl rigid substituents together with keeping the crescent shape of the molecule resulted in very high affinity for the minor groove of a six consecutive AT base pairs site. These data on structural requirements for minor groove DNA binding will help the rational design of porphyrin derivatives for selective targeting of quadruplex DNA versus double-stranded DNA.

Experimental Section

Materials and Methods. The following compounds were commercially available: NaOH (small beads) and piperidine (Fluka), nickel(II) chloride hexahydrate, nickel(II) acetate tetrahydrate, methyl tosylate, and 2,4,6-collidine (Aldrich), pyrrole, 4-(pyrid-2-yl)benzaldehyde, iodomethane, and DOWEX 1x8-200 resin (chloride form) (Acros), manganese(II) chloride (Riedel-de Haen). Thin layer chromatography (TLC) analysis was performed with Merck 60 F254 silica-coated aluminum plates. Sep-Pak C18 cartridges (Vac 20 cm^3, 5 g) were from Waters. DMF was dried over 4 Å molecular sieves. Potassium monopersulfate, $KHSO_5$ (triple salt 2 $KHSO_5$xK_2SO_4x$KHSO_4$, Curox) was from Interox. The oligonucleotides were purchased from Eurogentec (Belgium) and yeast tRNA (10 mg/mL) from Sigma. ^{1}H NMR spectra were recorded on Bruker Avance-300, and ARX-250 spectrometer with the residual solvent peak as internal calibration. Mass spectra were recorded either on a PerkinElmer SCIEX API 365 or Applied Biosystems Q TRAP. UV−visible spectra were recorded on a Hewlett-Packard 8452A spectrophotometer. Porphyrins were prepared according to literature procedures[7,11,48−50] with some

(27) Wang, P.; Ren, He, H.; Liang, F.; Zhou, X.; Tan, Z. *ChemBioChem* **2006**, *7*, 1155–1159.
(28) Weiner, P. K.; Langridge, R.; Blaney, J. M.; Schaefer, R.; Kollman, P. A. *Proc. Natl. Acad. Sci. U.S.A.* **1982**, *79*, 3754–3758.
(29) Lavery, R.; Pullman, B. *J. Biomol. Struct. Dyn.* **1985**, *2*, 1021–1032.
(30) Nguyen, B.; Neidle, S.; Wilson, W. D. *Acc. Chem. Res.* **2009**, *42*, 11–21.
(31) Schmid, N.; Behr, J. P. *Biochemistry* **1991**, *30*, 4357–4361.
(32) Pelton, J. G.; Wemmer, D. E. *Proc. Natl. Acad. Sci. U.S.A.* **1989**, *86*, 5723–5727.
(33) Ward, B.; Rehfuss, R.; Dabrowiak, J. C. *J. Biomol. Struct. Dyn.* **1987**, *4*, 685–695.
(34) Czarny, A.; Boykin, D. W.; Wood, A. A.; Nunn, C. M.; Neidle, S.; Zhao, M.; Wilson, W. D. *J. Am. Chem. Soc.* **1995**, *117*, 4716–4717.
(35) Kielkopf, C. L.; White, S.; Szewczyk, J. W.; Turner, J. M.; Baird, E. E.; Dervan, P. B.; Rees, D. C. *Science* **1998**, *282*, 111–115.
(36) Dervan, P. B.; Edelson, B. S. *Curr. Opin. Struct. Biol.* **2003**, *13*, 284–299.
(37) Kumar, D.; Veldhuyzen, W. F.; Zhou, Q.; Rokita, S. E. *Bioconjugate Chem.* **2004**, *15*, 915–922.
(38) Dervan, P. B. *Bioorg. Med. Chem.* **2001**, *9*, 2215–2235.
(39) Antonow, D.; Kaliszczak, M.; Kang, G. D.; Coffils, M.; Tiberghien, A. C.; Cooper, N.; Barata, T.; Heidelberger, S.; James, C. H.; Zloh, M.; Jenkins, T. C.; Reszka, A. P.; Neidle, S.; Guichard, S. M.; Jodrell, D. I.; Hartley, J. A.; Howard, P. W.; Thurston, D. E. *J. Med. Chem.* **2010**, *53*, 2927–2941.
(40) Tawar, U.; Jain, A. K.; Chandra, R.; Singh, Y.; Dwarakanath, B. S.; Chaudhury, N. K.; Good, L.; Tandon, V. *Biochemistry* **2003**, *42*, 13339–13346.
(41) Baguley, B. C. *Mol. Cell. Biochem.* **1982**, *43*, 167–181.
(42) Ward, B.; Skorobogaty, A.; Dabrowiak, J. C. *Biochemistry* **1986**, *25*, 6875–6883.
(43) Dabrowiak, J. C.; Ward, B.; Goodisman, J. *Biochemistry* **1989**, *28*, 3314–3322.
(44) Pitié, M.; Pratviel, G.; Bernadou, J.; Meunier, B. *Proc. Natl. Acad. Sci. U.S.A.* **1992**, *89*, 3967–3971.
(45) Arnaud, P.; Zakrzewska, K.; Meunier, B. *J. Comput. Chem.* **2003**, *24*, 797–805.
(46) Pitié, M.; Boldron, C.; Pratviel, G. *Adv. Inorg. Chem.* **2006**, *58*, 77–130.
(47) Pitie, M.; Pratviel, G. *Chem. Rev.* **2010**, *110*, 1018–1059.
(48) Bernadou, J.; Pratviel, G.; Bennis, F.; Girardet, M.; Meunier, B. *Biochemistry* **1989**, *28*, 7268–7275.
(49) Maraval, A.; Franco, S.; Vialas, C.; Pratviel, G.; Blasco, M. A.; Meunier, B. *Org. Biomol. Chem.* **2003**, *1*, 921–927.
(50) Fudickar, W.; Zimmermann, J.; Ruhlmann, L.; Schneider, J.; Roder, B.; Siggel, U.; Fuhrhop, J. H. *J. Am. Chem. Soc.* **1999**, *121*, 9539–9545.

modifications as detailed below (and in Supporting Information for the *meso*-5,10,15,20-tetrakis(4-*N*-methylpyridinumyl)porphyrins, namely, H_2-, Mn-, and Ni-TMPyP). Mass analyses were performed by the Mass Spectrometry Laboratory of ICSN-CNRS, Gif-sur-Yvette, France.

***meso*-5,10,15,20-Tetrakis(4-(pyrid-2-yl)phenyl)porphyrin.** 4-(Pyrid-2-yl)benzaldehyde (2.8 g, 15.3 mmol) was dissolved in propionic acid (72 mL), pyrrole (1 g, 15.6 mmol) was added, and the mixture was refluxed for 1 h in the dark. The solvent was evaporated and the residue was dried under a vacuum. The crude product was taken in DMF (50 mL) and filtered. The product was washed with DMF (50 mL) and diethylether (2 × 50 mL) and dried under a vacuum. Yield: 0.78 g (0.84 mmol, 22%) purple solid. ^{1}H NMR (250 MHz, CDCl3) δ 8.99 (s, 8H, pyrrole), 8.90 (d, J = 5 Hz, 4H, pyridine), 8.44 (d, J = 8 Hz, 8H, phenyl), 8.38 (d, J = 8 Hz, 8H, phenyl), 8.10 (d, J = 8 Hz, 4H, pyridine), 7.95 (ddd, J = 8, 8, 1 Hz, 4H, pyridine), 7.40 (dd, J = 8, 5 Hz, 4H, pyridine), −2.66 (s, 2H, NH). TLC $R_f \approx 0.20$ (SiO_2, $CH_3CN/H_2O/KNO_3$ sat. 8:1:1).

***meso*-5,10,15,20-Tetrakis(4-(*N*-methyl-pyridinium-2-yl)phenyl)-porphyrin tetrakis(trifluoroacetate).** Tetrakis(4-(pyrid-2-yl)phenyl)-porphyrin (200 mg, 0.22 mmol) was dissolved in DMF (20 mL) and excess iodomethane (4 mL) was added. The mixture was heated at 155 °C for 3 h and acetone (100 mL) was added. The resulting purple precipitate was filtered off, washed with acetone, chloroform, and diethyl ether. The product was purified on reverse phase C18 column (20 g), elution H_2O with 0.1% TFA then H_2O/CH_3CN (80:20) with 0.1% TFA. Yield: 210 mg (0,14 mmol, 66%) purple solid. ^{1}H NMR (300 MHz, DMSO-d_6) δ 9.33 (d, J = 6 Hz, 4H, pyridine), 9.04 (s, 8H, pyrrole), 8.84 (dd, J = 8, 8 Hz, 4H, pyridine), 8.55 (d, J = 8 Hz, 8H, phenyl), 8.48 (dd, J = 8, 1 Hz, 4H, pyridine), 8.33 (ddd, J = 8, 6, 1 Hz, 4H, pyridine), 8.19 (d, J = 8 Hz, 8H, phenyl), 4.53 (s, 12H, CH_3−N), −2.83 (s, 2H, NH). UV−vis (H_2O), λ max nm (ε M^{-1} cm^{-1}) 416 (410×10^3), 516 (15×10^3), 552 (7×10^3), 580 (5×10^3), 634 (3×10^3). HRES$^+$-MS m/z: calculated for $[C_{68}H_{54}N_8]^{4+}$ = 245.6112, found: 245.6106. TLC $R_f \approx$ 0.15−0.20 (SiO_2, $CH_3CN/H_2O/KNO_3$ sat. 8:1:1). ^{13}C NMR characterization of *meso*-5,10,15,20-tetrakis(4-(*N*-methyl-pyridinium-2-yl)phenyl)porphyrin tetrachloride is provided as Supporting Information.

***meso*-5,10,15,20-Tetrakis(4-(*N*-methyl-pyridinium-2-yl)phenyl)-porphyrinatomanganese(III) pentachloride (Mn-2).** Tetrakis-(4-(*N*-methyl-pyridinium-2-yl)phenyl)porphyrin tetrakis(trifluoroacetate) (49.6 mg, 0.035 mmol) was dissolved in aqueous 0.02 M NaOH (5 mL). Manganese(II) chloride (60.2 mg, 0.3 mmol) was dissolved in water (1 mL) and added to the porphyrin solution. The mixture was refluxed for 2 h. The reaction was monitored by UV−visible spectroscopy and was stopped when the Soret band shift was complete (from 416 to 466 nm, H_2O). Desalting of the porphyrin was performed by reverse phase chromatography on a C18 Sep-Pak cartridge (5 g, Waters) by elution with Milli-Q water followed by methanol containing 0.1% trifluoracetic acid. The collected fractions were evaporated to dryness and the product was taken in methanol. Anion exchange was performed on a DOWEX 1x8-200 resin column (chloride form, 6 g). The product was precipitated by the addition of diethyl ether, filtered, and washed with Et_2O. Yield: 33.1 mg (0.27 mmol, 78%) green purple solid. UV−vis (H_2O), λ max nm (ε M^{-1} cm^{-1}) 380 (55×10^3), 400 (56×10^3) 466 (96×10^3), 562 (12×10^3), 596 (8×10^3). HRES$^+$-MS m/z: calculated for $[C_{68}H_{52}MnN_8]^{5+}$ = 207.0739, found: 207.0723. TLC $R_f \approx$ 0.13 (SiO_2, $CH_3CN/H_2O/KNO_3$ sat. 8:1:1).

***meso*-5,10,15,20-Tetrakis(4-(*N*-methyl-pyridinium-2-yl)phenyl)-porphyrinatonickel(II) tetrachloride (Ni-2).** Tetrakis(4-(*N*-methyl-pyridinium-2-yl)phenyl)porphyrin tetrakis(trifluoroacetate) (51 mg, 0.03 mmol) was dissolved in aqueous 0.02 M NaOH (5 mL). Nickel(II) chloride hexahydrate (72 mg, 0.3 mmol) was dissolved in water (1 mL) and added to the porphyrin solution. The mixture was refluxed for 24 h. The reaction was monitored by UV−visible spectroscopy and was stopped when the Soret band shift was complete (from 438 to 412 nm, H_2O, acidic pH). Purification and counterion exchange were performed as described above for **Mn-2**. Yield: 27 mg (0.02 mmol, 67%) solid. ^{1}H NMR (400 MHz, DMSO-d_6), δ 9.38 (d, J = 6.1 Hz, 4H, pyridine), 8.96 (s, 8H, pyrrole), 8.82 (dd, J = 8, 8 Hz, 4H, pyridine), 8.43 (d, J = 7.6 Hz, 4H, pyridine), 8.35 (d, J = 8 Hz, 8H, phenyl), 8.30 (dd, J = 7, 7 Hz, 4H, pyridine), 8.14 (d, J = 8 Hz, 8H, phenyl), 4.48 (s, 12H, CH_3−N). UV−vis (H_2O), λ max nm (ε M^{-1} cm^{-1}) 284 (43×10^3), 412 (244×10^3) 524 (17×10^3). HRES$^+$-MS m/z: calculated for $[C_{68}H_{52}NiN_8]^{4+}$ = 259.5917, found: 259.5905. TLC $R_f \approx$ 0.23 (SiO_2, $CH_3CN/H_2O/KNO_3$ sat. 8:1:1).

Ni-1. A mixture of the non-metalated porphyrin H_2-1 (50 mg, 0.028 mmol; synthesis according to a previously published procedure),[11] nickel(II) acetate tetrahydrate (21 mg, 0.085 mmol), and 2,4,6-collidine (0.2 mL) was heated in DMF (1.5 mL) at 110 °C in the dark for 24 h. The reaction was monitored by UV−visible spectroscopy and was stopped when the Soret band shift was complete (from 447 to 414 nm, H_2O, acidic pH). The porphyrin was precipitated by addition of Et_2O (25 mL). The solution was centrifuged. The solid was dissolved in $MeOH/H_2O$ (4 mL, 1:1) and gently stirred with DOWEX 1x8-200 resin (chloride form) for 72 h. The resin was filtered and washed with MeOH, and the filtrate was evaporated and dried under a vacuum. Yield: 66 mg (0.017 mmol, 60%) red glossy solid. ^{1}H NMR (250 MHz, DMSO-d_6), δ 10.86 (s, 4H, NH), 9.17 (s, 4H, pyridine), 8.90 (d, J = 4.9 Hz, 4H, pyridine), 8.73 (s, 8H, pyrrole), 8.61 (d, J = 8 Hz, 4H, pyridine), 8.12 (m, 4H, pyridine), 8.02 (d, J = 8 Hz, 8H, phenyl), 7.91 (d, J = 8 Hz, 8H, phenyl), 4.39 (s, 12H, CH_3−N), 3.2−3.5 (CH_2, superimposed with water peak), 3.01 (m, 8H, CH_2). UV−vis (H_2O), λ max nm (ε M^{-1} cm^{-1}) 414 (110×10^3), 529 (9×10^3). HRES$^+$-MS m/z: calculated for $[C_{80}H_{72}N_{12}NiO_4]^{4+}$ = 330.6288, found: 330.6273.

Mn-1. This compound was prepared according to a previously published procedure (ref 11). HRES$^+$-MS m/z: calculated for $[C_{80}H_{72}N_{12}MnO_4]^{5+}$ = 263.9036, found: 263.9013.

Purification and Labeling of the Oligonucleotides. Purification of oligonucleotides was performed by electrophoresis on 20% polyacrylamide denaturing gel (7 M urea). DNA concentration was determined by UV absorbance measurements at 260 nm taking the supplier extinction coefficient value for each oligonucleotide. The 5′-end of oligonucleotides was ^{32}P-labeled using standard procedures with T4 polynucleotide kinase (Sigma) and [γ-^{32}P]ATP (Perkin-Elmer).

Oxidative Cleavage of Double-Stranded 19-mer. The cleavage reactions on double-stranded DNA were performed on a 19-mer duplex which was 5′-^{32}P-end labeled on one strand (10^5 cpm). Annealing of the two 19-mer single-strands was achieved in 40 mM phosphate buffer pH 7 and 100 mM NaCl by heating at 90 °C for 5 min followed by slow cooling to room temperature. A typical experiment was performed at a duplex final concentration of 1 μM, in 40 mM phosphate buffer pH 7.0 and 100 mM NaCl. Double-stranded DNA was incubated with Mn-TMPyP (final concentration of 0.5 or 2 μM) in the absence or in the presence of competitor porphyrin during 1 h for the system to come to equilibrium. Cleavage reactions were initiated by the addition of a freshly prepared solution of $KHSO_5$ at a final concentration of 250 μM or 1 mM. Total reaction volume was 10 μL. After 1 or 10 min at 4 °C, the oxidation reactions were stopped by the addition of *N*-(2-hydroxyethyl)piperazine-*N*′-ethanesulfonic acid (Hepes) buffer (100 mM, final concentration). DNA was precipitated by successive additions of 1 μL of 3.5 M sodium acetate buffer pH 5.2, 1 μL of 1 M NaCl, 1 μL of yeast tRNA (10 mg/mL), and 100 μL of cold ethanol. After centrifugation (15 min, 4 °C, 12×10^3 rpm), the DNA pellet was washed with cold ethanol and dried under a vacuum. The dried DNA pellet was either solubilized in deionized formamide with marker dyes for direct electrophoresis analysis or dissolved in 100 μL of 1 M piperidine, and incubated at 90 °C for 30 min. After piperidine treatment, several steps of

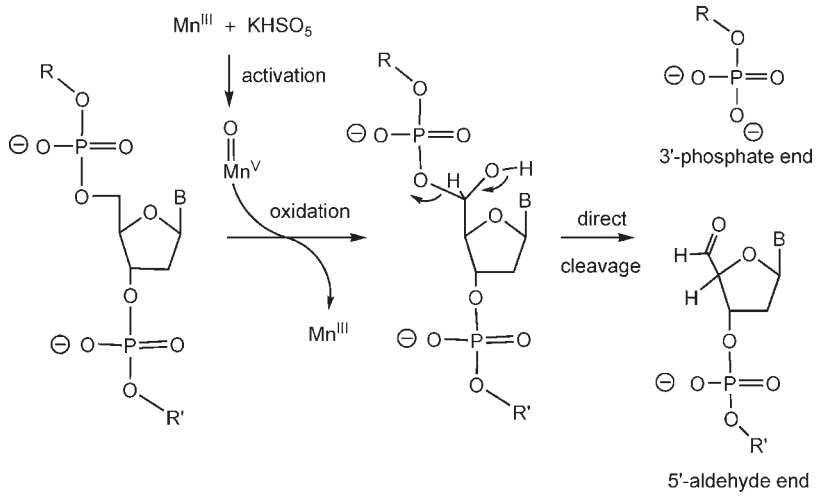

Figure 1. Molecular mechanism of DNA cleavage by the chemical nuclease, Mn-TMPyP/$KHSO_5$. Hydroxylation of C5′-H bond of deoxyribose leads to direct cleavage of a DNA strand in two fragments with 5′-aldehyde or 3′-phosphate termini. The porphyrin macrocycle is omitted for clarity.

lyophilization were performed before dilution of the dry DNA pellet in deionized formamide with marker dyes.

Polyacrylamide Gel Electrophoresis. The DNA samples were heated 2 min at 90 °C, chilled in ice, and loaded on a 20% denaturing polyacrylamide gel (7 M urea). Migration lasted 3 h at 2000 V in tris(hydroxymethyl)aminomethane-borate 9 mM pH 8 buffer, 0.03 mM EDTA. The DNA fragments were visualized and quantified by phosphorimagery (Biorad PMI).

Surface Plasmon Resonance. Two 5′-biotinylated hairpin DNA duplexes were grafted on the surface of a streptavidine sensor chip, an AT-rich duplex, 5′-biot-CGAATTATAAATCGTCTCCGATTTATAATTCG and a GC-rich duplex, 5′-biot-GGCATAGTGCGTGGGCGTTAGCTTTTGCTAACGCCCACGCACTATGCC. Details of the experimental procedure are provided as Supporting Information.

Results and Discussion

The pentacationic manganese(III) porphyrin, Mn-TMPyP, in the presence of an oxygen atom donor such as $KHSO_5$ (oxone) soluble in water at physiological pH transforms to a high-valent manganese(V)-oxo species (Mn^V-oxo).[51] This activated species is a powerful oxidant and an efficient artificial nuclease. It is able to mediate direct DNA cleavage through hydroxylation of the minor groove oriented 5′-CH bond of deoxyribose thanks to a very precise positioning of the porphyrin within the minor groove of DNA. The oxidation reaction consists of oxygen atom transfer from the oxo-form of the metalloporphyrin to the C5′-carbon of deoxyribose (Figure 1). The resulting cleavage products are 3′-phosphate and 5′-aldehyde ending DNA strands. As can be seen in Figure 1, the oxidation reaction is catalytic in nature since the Mn(III) porphyrin regenerates in the course of the reaction.[46,47,51] The preferred binding and cleavage site of Mn-TMPyP/$KHSO_5$ consists of three consecutive AT base pairs, referred to as an $(AT)_3$ box.[44−47,52] The binding constant of Mn-TMPyP for this particular site is very high: 10^6-10^7 M^{-1}.[7,23,43] In the absence of $KHSO_5$, Mn-TMPyP binds to DNA but is unable to perform oxidative cleavage. The activation and cleavage reaction of this chemical nuclease is extremely rapid and takes place in less than a minute once $KHSO_5$ is added. Activation of Mn-TMPyP by $KHSO_5$ is possible while it is located inside the minor groove of DNA.[45] DNA attack may occur on either strand, and a 3′-shifted DNA cleavage results.[44−47,52] The exquisite positioning of the Mn^V-oxo in the vicinity of its target leads to a very precise hydroxylation of 5′-CH of deoxyribose of the nucleotide unit that is located immediately 3′ to the last base pair of the $(AT)_3$ site (Figure 2). The high affinity and high cleavage efficiency of Mn-TMPyP/$KHSO_5$ in an $(AT)_3$ site in a DNA duplex is a convenient tool to study the interaction of competitors for the same site on DNA since the presence of Mn-TMPyP in the minor groove of an $(AT)_3$ box is readily revealed by DNA cleavage at this site. Displacement of Mn-TMPyP from this site by the binding of a competitor ligand will lower or abolish DNA cleavage. DNA cleavage was assayed on two different double-stranded oligonucleotides. The chosen 19-mer duplex oligonucleotides contained three (ds19−3AT) and six (ds19−6AT) consecutive AT base pairs, that is, one and four overlapped $(AT)_3$ box(es), respectively (Figure 2). The numbering of oligonucleotide bases starts at the 5′-position of the upper strand.

The structures of the used porphyrins are shown in Figure 3. The manganese(III) and nickel(II) complexes of three different cationic porphyrins were prepared. Mn-TMPyP and Ni-TMPyP,[48,49] **Mn-2** and **Ni-2**,[50] were prepared with modifications of previously reported procedures. **Mn-1** and **Ni-1** were prepared according to ref 11. Metalation with nickel was performed following classic protocols. The manganese(III) porphyrin, **Mn-1**, was previously reported to be a specific quadruplex DNA binder with no affinity for double-stranded DNA.[11] **Ni-2** and **Mn-2** are new porphyrins in the field of DNA targeting.[50]

Competitive Interaction of Porphyrins in the Minor Groove of Three Consecutive AT Base Pairs. The cleavage of ds19−3AT duplex by Mn-TMPyP/$KHSO_5$ is shown in Figure 4. 5′-Labeled double-stranded DNA was incubated with Mn-TMPyP for 1 h. After this equilibrium step allowing Mn-TMPyP to interact with DNA, $KHSO_5$ was added to activate the manganese porphyrin and the cleavage reaction lasted 1 min (Figures 4A and S2, Supporting Information) or 10 min (Figure 4B). Control experiments consisting of DNA incubation with either $KHSO_5$ (lane 1) or Mn-TMPyP

(51) Meunier, B.; Robert, A.; Pratviel, G.; Bernadou, J. In *The Porphyrin Handbook*; Kadish, K. M., Smith, K. M., Guillard, R., Eds.; Academic Press: San Diego, 2000; Vol. *4*, p 119−187.

(52) Wietzerbin, K.; Muller, J. G.; Jameton, R. A.; Pratviel, G.; Bernadou, J.; Meunier, B.; Burrows, C. J. *Inorg. Chem.* **1999**, *38*, 4123–4127.

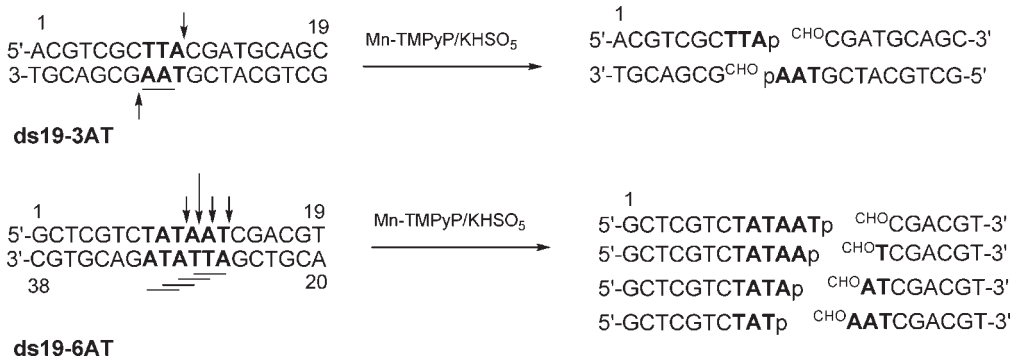

Figure 2. Double-stranded 19-mer oligonucleotides used. The binding site of Mn-TMPyP consisting of $(AT)_3$ boxes are underlined and the cleavage sites of Mn-TMPyP/$KHSO_5$ are also indicated (arrow). One site of cleavage is present on duplex DNA with only three consecutive AT base pairs (ds19−3AT). Duplex containing six consecutive AT base pairs (ds19−6AT) shows four sites of cleavage. The four products of the two single-stranded cleavage reaction are shown for ds19−3AT, which contains only one $(AT)_3$ binding site for the nuclease. For clarity, only the single-stranded cleavage products of the upper strand are shown for the ds19−6AT duplex. The "p" and "CHO" marks refer to 3′-phosphate and 5′aldehyde termini, respectively. The numbering of the nucleoside units of oligonucleotides is also indicated.

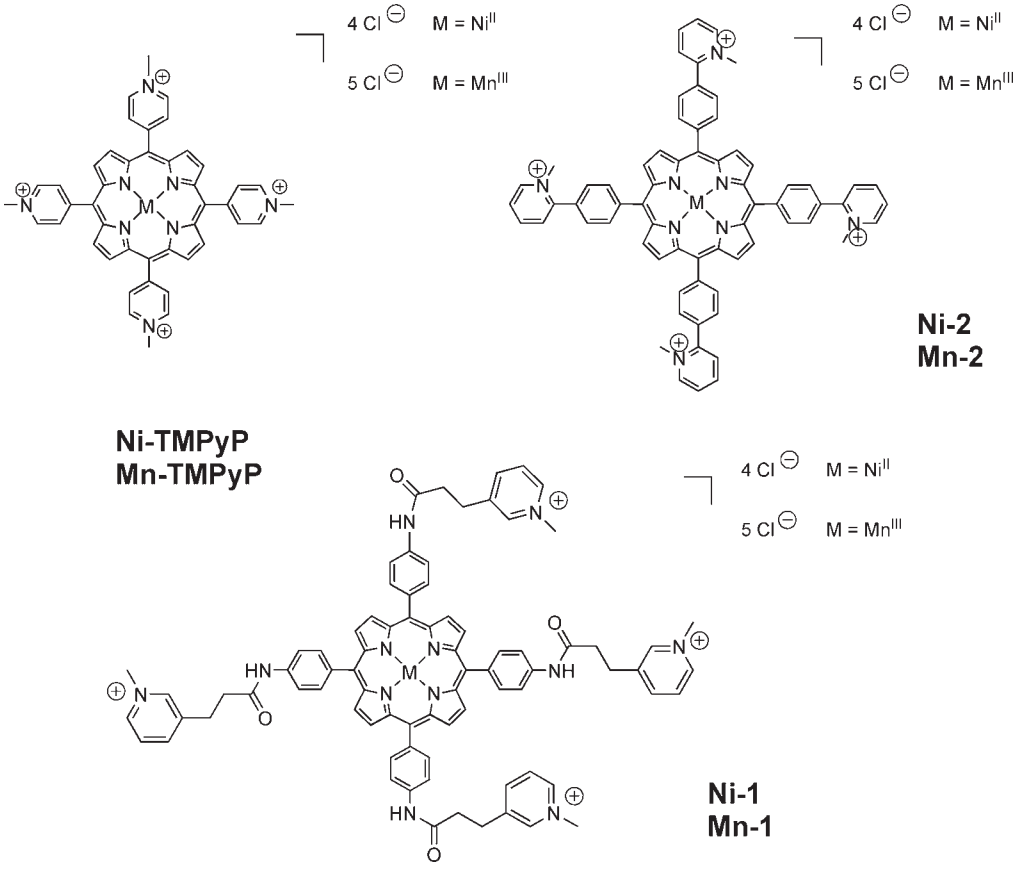

Figure 3. Structure of the porphyrins. Nickel(II) porphyrins bear four chloride counterions. Manganese(III) porphyrins bear two water molecules as axial ligands (omitted for clarity) on the central manganese ion and five chloride counterions.

(not shown) displayed intact, full-length DNA at the top of the gel. Besides, the oxidation reaction of the activated species of Mn-TMPyP within the minor groove of the $(AT)_3$ box generated the expected 5′-labeled-ACGTCGCTTA-3′-phosphate fragment (arrow, Figure 4). The amount of cleavage proved higher after 10 min compared to 1 min of reaction, and reached 90 and 20% yield, respectively. This yield of cleavage provides the control reactions with no inhibition.

For competition experiments, the nickel porphyrins were allowed to incubate together with Mn-TMPyP during the equilibrium step. The concentration of competitor porphyrin increased from 2 to 50 μM, which corresponded to 1−25 mol equiv with respect to Mn-TMPyP. After addition of $KHSO_5$, Ni-TMPyP (5 μM, 2.5 mol equiv) inhibited 90% of the cleavage reaction when the reaction was stopped after 1 min (Figure 4A). When the oxidation reaction was allowed to proceed during 10 min, the same extent of inhibition was achieved with a concentration of 10 μM (5 mol equiv of Ni-TMPyP with respect to Mn-TMPyP, Figure 4B, lane 11). This data are in accordance with the affinity of Ni-TMPyP for the DNA minor groove

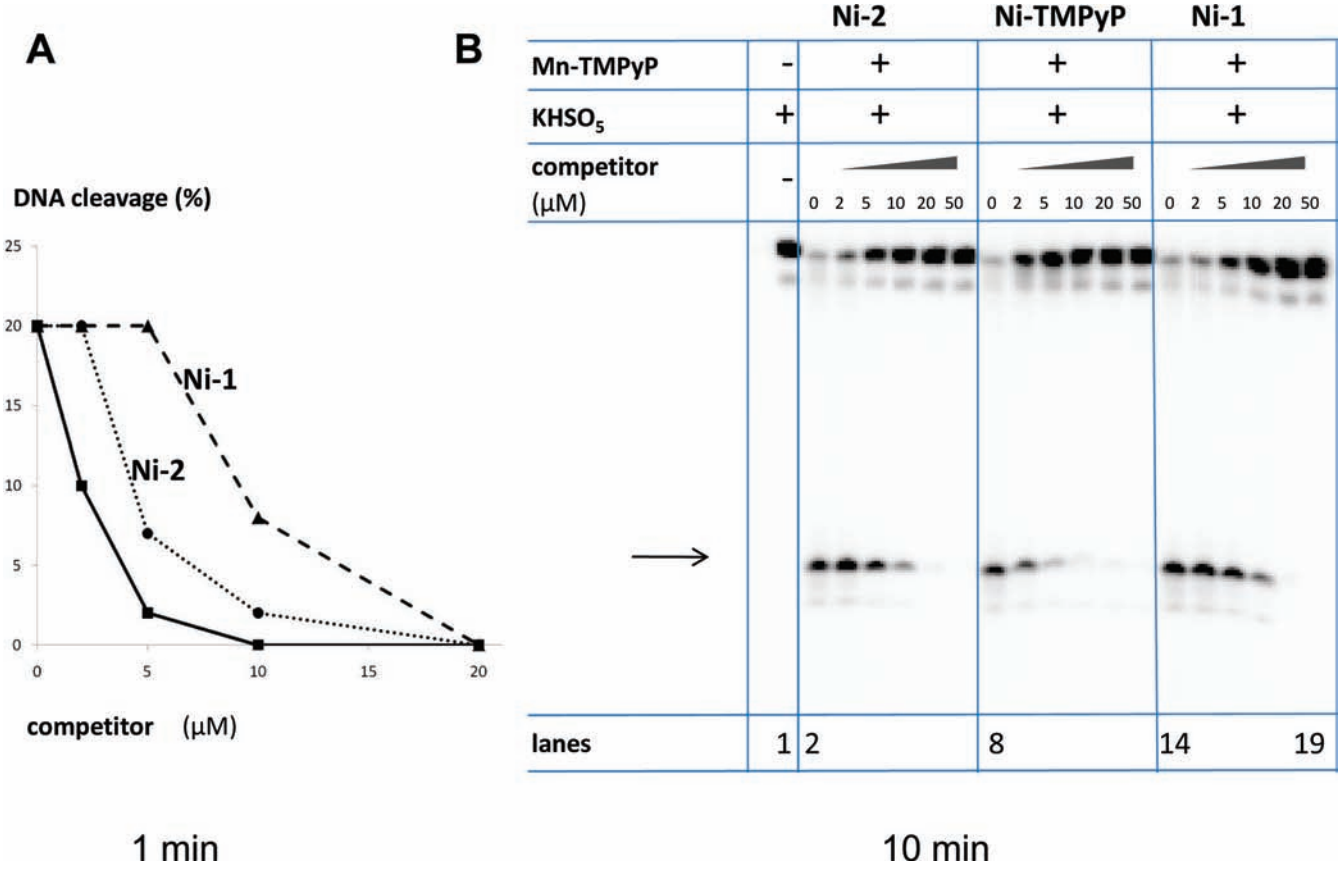

Figure 4. Polyacrylamide gel electrophoresis analysis of the cleavage of double-stranded ds19−3AT by Mn-TMPyP/$KHSO_5$ in the presence of competitor nickel(II) porphyrins, Ni-TMPyP, **Ni-1** and **Ni-2**. The duplex oligonucleotide (1 μM) was incubated with Mn-TMPyP (2 μM) in 40 mM phosphate buffer pH 7.0, 100 mM NaCl and in the presence of an increasing amount of competitor porphyrin (2, 5, 10, 20, 50 μM, i.e., 1, 2.5, 5, 10, and 25 equiv, respectively, with respect to Mn-TMPyP) during 1 h at 0 °C. Addition of $KHSO_5$ (1 mM) activated Mn-TMPyP and started the cleavage reaction, which lasted either 1 min (A) or 10 min (B) at 0 °C. Controls consisted of incubation of duplex DNA with 1 mM $KHSO_5$ at 0 °C (lane 1). DNA cleavage by Mn-TMPyP/$KHSO_5$ for 10 min of reaction in the absence of competitor corresponds to lanes 2, 8, and 14. The cleaved fragment (arrow) is the single stranded 5′-labeled 10-mer 5′-ACGTCGCTTA-3′-phosphate oligonucleotide. Quantification of this fragment is provided in A for 1 min reaction with Ni-TMPyP (■), **Ni-1** (▲), and **Ni-2** (●).

being lower than that of Mn-TMPyP due to the smaller number of positive charges of Ni-TMPyP carried by the porphyrin.[7]

The two other porphyrins, **Ni-1** and **Ni-2**, were less efficient in inhibiting DNA cleavage of Mn-TMPyP/$KHSO_5$ nuclease compared to the nickel homologue of Mn-TMPyP. Complete inhibition of DNA cleavage was achieved with 20 μM of **Ni-2** (1 min) and with 50 μM (10 min, Figure 4B, lane 7) and 20 μM of **Ni-1** (1 min) and 50 μM (10 min, Figure 4B, lane 19).

The results of the inhibition of the 1 and 10 min reactions led to the same conclusion. Compared to Ni-TMPyP, **Ni-1** and **Ni-2** were poor inhibitors of Mn-TMPyP/$KHSO_5$ nuclease in the $(AT)_3$ binding site on DNA. **Ni-2** seemed to be better than **Ni-1**. It was concluded that these two porphyrin derivatives did not show significant affinity for the minor groove of a 3 AT site.

Competitive Interaction of Porphyrins in the Minor Groove of Six Consecutive AT Base Pairs. In the same way as described for the previous duplex, the Mn-TMPyP/$KHSO_5$ nuclease was allowed to cleave ds19−6AT duplex in the presence of competitor nickel porphyrins. The ds-19−6AT duplex contains six AT base pairs in a row and therefore has four potential overlapped $(AT)_3$ binding sites for Mn-TMPyP. The duplex was 5′-labeled on the upper strand (Figure 5A). After preincubation of the porphyrins with DNA, the addition of $KHSO_5$ started the cleavage reaction that was allowed to proceed for 10 min. As expected, ds19−6AT afforded four cleavage fragments. One of them (resulting from the binding of the nuclease in the 5′-TAA box) appeared as a higher cleavage spot (arrows, Figure 5). Under the present experimental conditions, the reference cleavage reaction reached 20% yield (lanes 3, 9 and 15, Figure 5). The nuclease system was four times less concentrated compared to the reaction analyzed in Figure 4. The concentration of competitor porphyrin increased from 2 to 50 μM, that is, from 4 to 100 mol equiv with respect to Mn-TMPyP.

Under the used experimental conditions Ni-TMPyP porphyrin totally inhibited the cleavage of Mn-TMPyP/$KHSO_5$ at 10 μM concentration (20 mol equiv with respect to Mn-TMPyP) (lane 12, Figure 5) and effected 50% of inhibition at 5 μM (10 mol equiv) (lane 11). As in the case of ds19−3AT, the affinity of **Ni-1** and **Ni-2** porphyrins can be evaluated with respect to the standard Ni-TMPyP. **Ni-1** porphyrin inhibited the cleavage reaction once its concentration reached 50 μM (100 mol equiv) (lane 20, Figure 5). Finally, **Ni-2** proved to interact in the minor groove of the six AT region in a stronger manner than Ni-TMPyP. It came out as the best inhibitor and was capable of preventing DNA cleavage at 5 μM concentration (10 mol equiv) (lane 5, Figure 5).

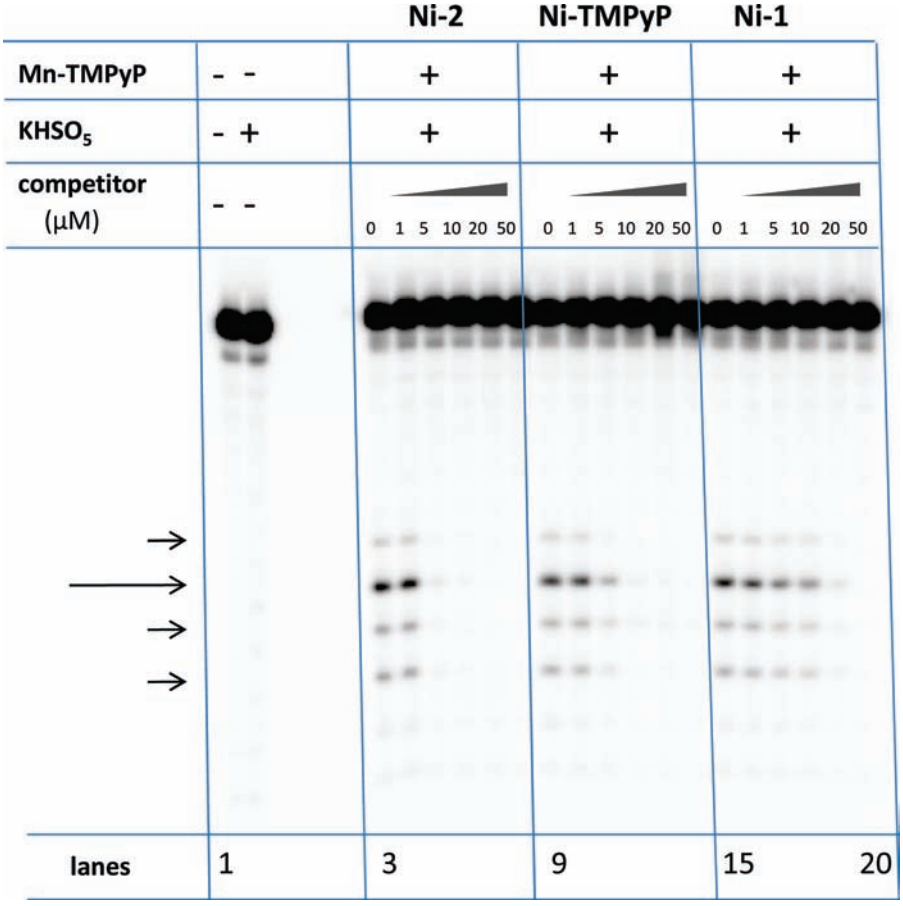

Figure 5. Polyacrylamide gel electrophoresis analysis of the cleavage of double-stranded ds19−6AT by Mn-TMPyP/$KHSO_5$ in the presence of competitor nickel(II) porphyrins, **Ni-2** (lanes 4−8), Ni-TMPyP (lanes 10−14) and **Ni-1** (lanes 16−20). The duplex oligonucleotide (1 μM) was incubated with Mn-TMPyP (0.5 μM) in 40 mM phosphate buffer pH 7, 100 mM NaCl and in the presence of increasing amounts of competitor porphyrin (1, 5, 10, 20, and 50 μM, i.e., 2, 10, 20, 40, and 100 equiv, respectively, with respect to Mn-TMPyP) during 1 h at 0 °C. Addition of $KHSO_5$ (250 μM) activated Mn-TMPyP and started the cleavage reaction, which lasted 10 min at 0 °C. Controls consisted of incubation of duplex DNA without and with 250 μM $KHSO_5$ at 0 °C, lanes 1 and 2, respectively. DNA cleavage by Mn-TMPyP/$KHSO_5$ in the absence of competitor can be seen in lanes 3, 9, and 15. The major DNA fragment is the 5′-labeled single-stranded 12-mer 5′-GCTCGTCTATAA-3′-phosphate oligonucleotide.

Thus, this experiment provided, for the six AT base pairs site, a different rank between the porphyrins: **Ni-2** > Ni-TMPyP > **Ni-1**.

In conclusion, **Ni-1** porphyrin carrying flexible bulky substituents was unable to bind in the minor groove of short (three AT base pairs) and long (six AT base pairs) regions of AT sequences in comparison with Mn-TMPyP and Ni-TMPyP. The weak cleavage inhibition of **Ni-1**, which is observed with more than 40 mol equiv may be due to nonspecific interactions of the competitor porphyrin with DNA (electrostatic interactions). This confirms the weak affinity reported for **Mn-1** derivatives for double-stranded DNA.[11] Surprisingly, **Ni-2** porphyrin with rigid and intermediate in length substituents, proved a better ligand than Ni-TMPyP for the minor groove of the six AT track, although it was unable to bind strongly to the minor groove of the smaller $(AT)_3$ site.

Therefore, to know whether the manganese derivative, **Mn-2**, could be a better DNA cleaving reagent than Mn-TMPyP at the particular DNA sequence consisting of six consecutive AT base pairs it was incubated with $KHSO_5$ and tested as a DNA cleaver.

Oxidation Reaction of the Manganese Porphyrins, Mn-1 and Mn-2 Associated to $KHSO_5$ toward DNA. The ds19−6AT duplex was 5′-labeled on the upper strand (Figure 6A) and tested with individual manganese porphyrin. Different concentrations of manganese porphyrin were tested. Mn-TMPyP was reacted at 0.5 μM, while **Mn-1** and **Mn-2** were reacted at 0.5, 2.5, and 12.5 μM concentration. After the binding equilibrium between the manganese porphyrin and DNA was reached, $KHSO_5$ was added in the reaction medium and the oxidation reaction was allowed to proceed for 10 min. The standard cleavage reaction mediated by Mn-TMPyP/$KHSO_5$ is shown again in lanes 1 (Figure 6). **Mn-1** did not generate any direct cleavage fragments (lanes 2−4, Figure 6), which is consistent with the fact that the nickel derivative of this porphyrin, **Ni-1**, was unable to interact significantly in the minor groove of the duplex. However, **Mn-2** associated to $KHSO_5$ proved not to be an efficient nuclease although **Ni-2** was able to strongly bind to the minor groove of a six AT base pairs site. Some cleavage products identical to those generated by Mn-TMPyP/$KHSO_5$ could be observed but in much smaller amounts (lanes 5−7, Figure 6). The reactive center of **Mn-2**, the Mn^V-oxo entity, was not properly positioned for efficient hydroxylation at the 5′-position of deoxyribose. Unfortunately, this work cannot give any indication of the precise binding mode of **Mn-2**.

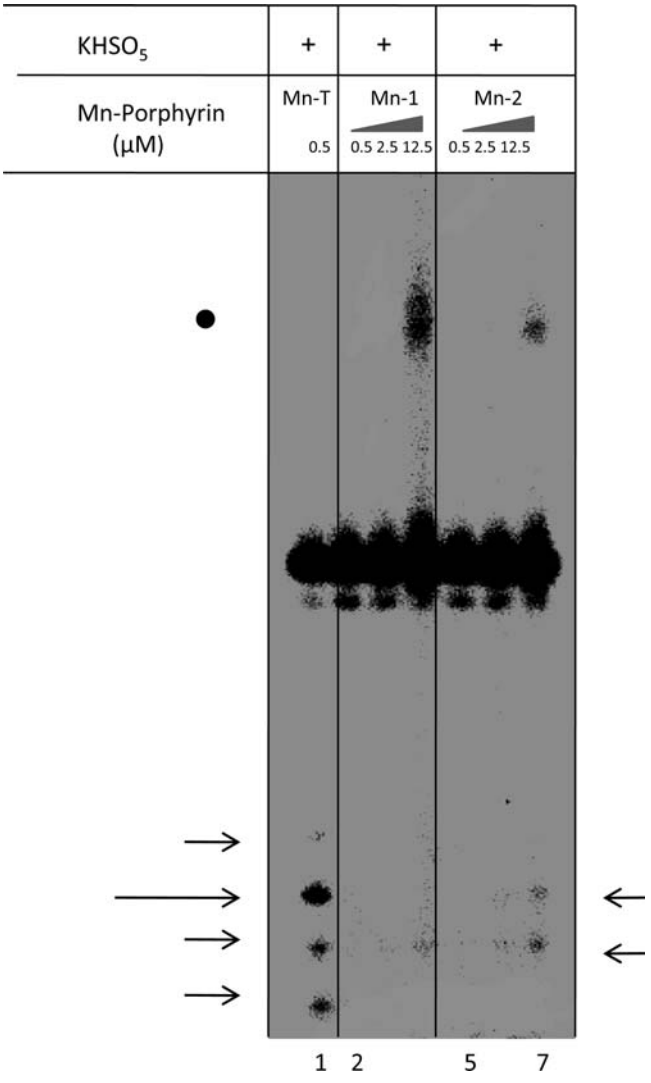

Figure 6. Polyacrylamide gel electrophoresis analysis of the cleavage of double-stranded ds19−6AT by Mn-TMPyP, **Mn-1** and **Mn-2**, in the presence of $KHSO_5$. Manganese porphyrins were preincubated with labeled duplex during 1 h at 0 °C in 40 mM phosphate buffer pH = 7.0, NaCl 100 mM. Addition of $KHSO_5$ (250 μM) started the oxidation reaction, which lasted 10 min at 0 °C. Mn-TMPyP was tested at 0.5 μM (lane 1) while **Mn-1** (lanes 2−4) and **Mn-2** (lanes 5−7) concentrations were 0.5, 2.5, and 12.5 μM. T stands for TMPyP. Slower migrating material is marked (●). Cleavage fragments are indicated by arrows.

Nevertheless, under oxidative conditions, **Mn-1** and **Mn-2** porphyrin derivatives were not inactive against DNA. Mainly **Mn-1**, and to a lesser extent **Mn-2**, led to a broadening of the full-length DNA band and to the formation of slow migrating material above the full-length DNA (●) (Figure 6). These effects appeared only at a high concentration (12.5 μM) of **Mn-1** and **Mn-2**. The distinct slow migrating band was absent when **Ni-1** and **Ni-2** were used as competitors for Mn-TMPyP/$KHSO_5$ (not shown). The formation of retarded material cannot be accounted for some noncovalent interactions between the cationic porphyrins and DNA because it is clearly $KHSO_5$ dependent, as will be shown in Figure 7.

The slow migrating material was analyzed on the two strands of the duplex oligonucleotide and subjected to alkaline treatment in order to gain some insight into the molecular mechanism leading to its formation. Figure 7 shows the polyacrylamide gel analysis of the reaction mixtures of ds19−6AT incubated with Mn-TMPyP/$KHSO_5$ and **Mn-1**/$KHSO_5$ systems. The analysis of the oxidative reactions through the 5′-end labeling of the upper and the lower strand of the duplex are shown Figure 7, panels A and B, respectively. Slower migrating material was observed on the two strands of the duplex with **Mn-1** (10 μM) in the presence of $KHSO_5$ (lanes 4 and 16, Figure 7). One can note here two different slow migrating bands instead of one in Figure 6. The second and slower migrating band (○), lanes 4 and 16, was in a lower amount compared to the other one (●). The retarded products migrated at a distance corresponding to the position of a standard 5′-labeled single-stranded 39-mer oligonucleotide (○) and a 5′-labeled single-stranded 27-mer oligonucleotide (●) of random sequences (not shown). In the absence of $KHSO_5$, the two slower migrating bands were absent (lanes 3 and 15, Figure 7). They proved unstable upon piperidine treatment (lanes 10 and 22, Figure 7). Alkaline treatment gave rise to cleavage products comigrating with the fragments of the G-lane of Maxam and Gilbert sequencing reaction (not shown). They may arise both from the slow migrating material as well as from the damaged full-length DNA.

Thus, **Mn-1** porphyrin mediated oxidative DNA damage at G residues in the presence of $KHSO_5$. The slow migrating products may consist either of cross-links between the two strands of the DNA duplex or of DNA/porphyrin covalent adducts due to guanine oxidation. Guanine oxidation by Mn^{III}-porphyrin/$KHSO_5$ is well documented.[46,53−55] Manganese porphyrins activated by $KHSO_5$ are able to mediate one and two electron oxidation of guanine.[55] These mechanisms of oxidation may account for the formation of DNA/DNA cross-links or porphyrin/DNA adducts. Furthermore, oxidative damage at guanine is often associated with a broadening of the full-length DNA band on electrophoresis gels implying that guanine oxidation, not associated with slower migrating material, was also possible. Oxidative chemistry mediated by **Mn-1**/$KHSO_5$ may occur at any guanine position on the 19-mer DNA. The smaller fragments of both DNA strands were not observed under the chosen electrophoresis conditions.

In the presence of $KHSO_5$, a Mn^V-oxo species is likely to form with a similar yield with the three porphyrins, namely, Mn-TMPyP, **Mn-1** and **Mn-2**. The three Mn^V-oxo should be endowed with the same catalytic oxidation capacity. However, the efficiency of DNA damage and the nature of the oxidation products depend on the interaction of the porphyrin with DNA. When the activated species (Mn^V-oxo) interacts inside the minor groove in a suitable position with respect to deoxyriboses, hydroxylation of sugar carbon occurs. This is the key of the high efficiency of Mn-TMPyP/$KHSO_5$ nuclease at $(AT)_3$ sites where it is active at very low concentrations. However, it has been demonstrated that when the Mn^V-oxo species of a porphyrin derivative is not in close contact with CH

(53) Pratviel, G.; Meunier, B. *Chem.—Eur. J.* **2006**, *12*, 6018–6030.
(54) Mourgues, S.; Kupan, A.; Pratviel, G.; Meunier, B. *ChemBioChem* **2005**, *6*, 2326–2335.
(55) Makarska, M.; Pratviel, G. *J. Biol. Inorg. Chem.* **2008**, *13*, 973–979.

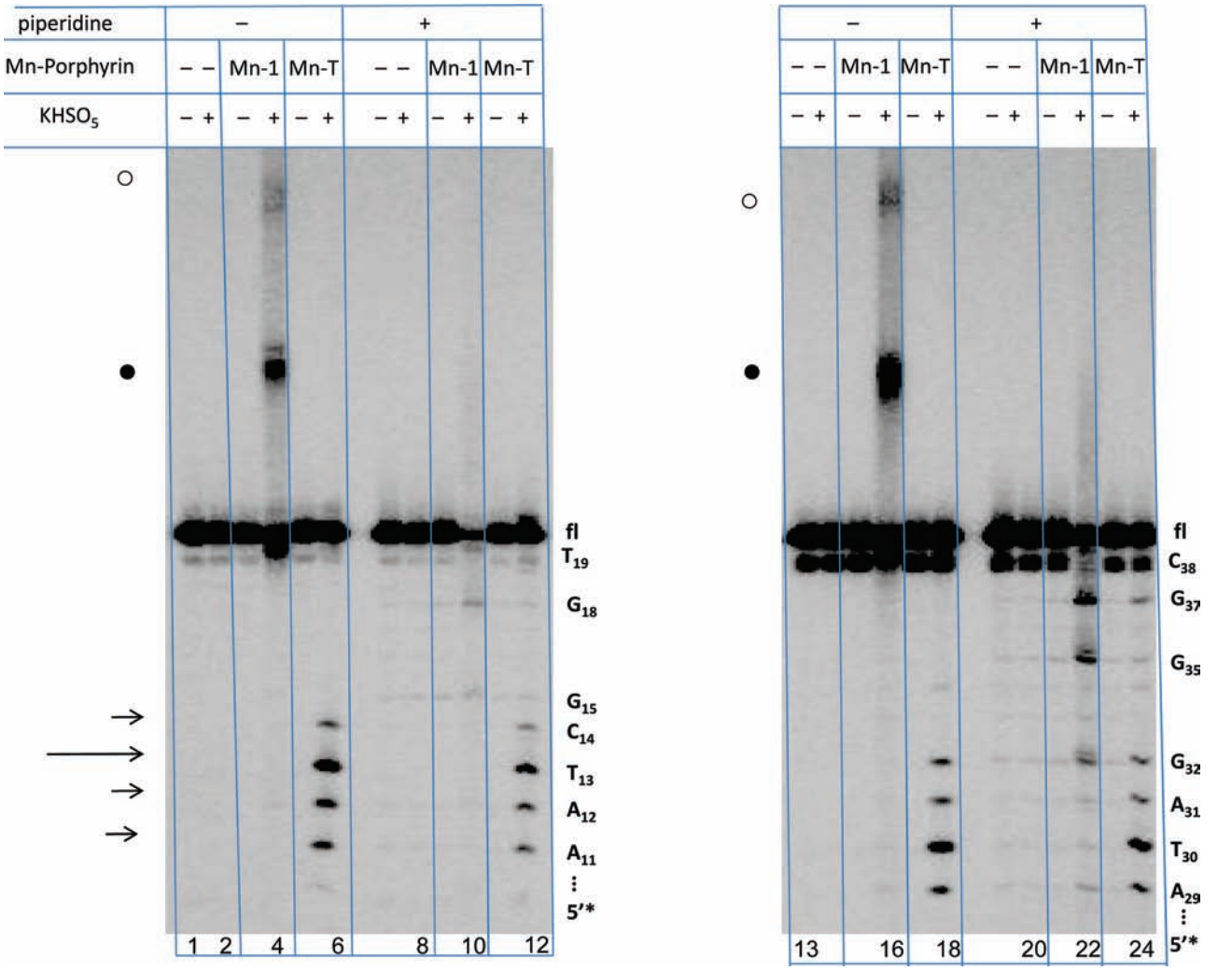

Figure 7. Polyacrylamide gel electrophoresis analysis of the cleavage of double-stranded ds19−6AT by Mn-TMPyP and **Mn-1** associated with $KHSO_5$. The 5′-labeled upper strand of the duplex was analyzed in the left part of the gel. The complementary 5′-labeled strand was analyzed in the right part of the gel. Mn-TMPyP (0.5 μM) and **Mn-1** (10 μM) were preincubated with labeled duplex during 1 h at 0 °C in 40 mM phosphate buffer pH = 7.0, NaCl 100 mM. Addition of $KHSO_5$ (250 μM) started the oxidation reaction, which lasted 10 min at 0 °C. The samples were analyzed either directly at the end of the reaction (lanes 1−6 and 13−18) or after piperidine treatment (alkali labile sites) (lanes 7−12 and 19−24). The marks (●, ○) indicate slower migrating materials. T stands for TMPyP. DNA fragments are marked according to the migration of Maxam and Gilbert sequencing lanes. Direct cleavage fragments mediated by Mn-TMPyP/$KHSO_5$ nuclease (without alkaline treatment) are shown by arrows. The cleavage fragments of the contaminating C_{38} and T_{19} bands are the same as those of the full-length DNA(fl).

bonds of deoxyriboses, the activated form of the manganese porphyrin instead reacts by an electron transfer mechanism.[54] The most oxidizable bases of DNA, namely, guanine bases, become the site of DNA damage.[46,54] Guanine oxidation by electron transfer is not as demanding as deoxyribose hydroxylation in terms of the distance between the Mn^V-oxo and DNA. Since **Mn-1** is a pentacationic porphyrin, it may approach DNA through electrostatic interactions with the phosphate groups. Additionally, in the case of the 19-mer duplex used in the present study, it may interact by $\pi-\pi$ stacking with the last base pair of the short duplex. Thus, from these two nonspecific binding modes (electrostatic interactions with phosphates or stacking with the last base pair of the duplex), **Mn-1** activated into a Mn^V-oxo species by $KHSO_5$ was able to mediate guanine oxidation, which was at the origin of the formation of either DNA/DNA cross-links or DNA/porphyrin covalent adducts. However, this oxidative degradation of DNA is only observed at high porphyrin concentration due to a low affinity binding constant between **Mn-1** and DNA.[11] **Mn-2** behaved in an intermediate manner compared to Mn-TMPyP and **Mn-1**. It was only capable of faint cleavage at the minor groove of DNA at the six AT site compared to Mn-TMPyP, and mediated less guanine damage than **Mn-1**. The behavior of **Mn-2** toward oxidative DNA damage may be interpreted in terms of a reduced availability of porphyrin for guanine damage due to binding (cleavage-inactive) of part of the porphyrin in the six AT site.

In summary, the manganese porphyrins **Mn-1** and **Mn-2** activated by $KHSO_5$ to oxidative reagents were unable to mediate efficient DNA damage at the six AT site. This result was not surprising in the case of **Mn-1** since **Mn-1**[11] and **Ni-1** (this work) were known to be poor double-stranded DNA ligands. However, **Mn-2** was not expected to be a sluggish reagent since **Ni-2** was shown to be a strong ligand for the minor groove of long AT sequences. Actually, the very low reactivity of **Mn-2** might be explained

Table 1. Porphyrin Binding Constants to Double-Stranded DNA Measured by SPR

	AT DNA	GC DNA
Mn-TMPyP	$0.5 \times 10^7\ M^{-1}$	–[a]
Mn-1	–	–
Mn-2	$6 \times 10^7\ M^{-1}$	–

[a] No binding (–).

by an unsuitable positioning of the Mn^V-oxo entity with respect to CH bonds of deoxyriboses without necessarily excluding a tight binding of the porphyrin in the minor groove of the long AT sequence. Guanine oxidative damage at high porphyrin concentration reveals weak and nonspecific interactions of these cationic porphyrins with DNA (negative phosphate groups and/or stacking interaction with the terminal base pairs).

Binding Affinity of Manganese Porphyrins for AT-rich and GC-rich Duplexes Measured by SPR. The competition studies did not allow the determination of the binding affinity of the manganese derivatives for DNA. Thus, the binding capacity of the manganese porphyrins for AT-rich and GC-rich DNA was assayed by surface plasmon resonance (SPR). Although SPR does not give any information on the mode of binding, on the opposite to previous competition studies, it gives access to the affinity binding constant of a ligand toward a target. Two 5′-biotinylated hairpin DNA duplexes were grafted on the surface of sensor chip, an AT- and a GC-rich duplex. The results confirm the absence of binding of **Mn-1** to the two types of DNAs, the selective binding of Mn-TMPyP on AT-rich DNA and the high binding affinity of **Mn-2** to AT-rich DNA (Table 1).

Conclusions

Ni-TMPyP and Mn-TMPyP porphyrins, carrying four *N*-methylpyridiniumyl substituents, are endowed with a high affinity for the minor groove of DNA ($K_A \sim 10^6 - 10^7\ M^{-1}$).[23,43] The minimum number of consecutive AT base pairs for this strong interaction to take place is only three AT base pairs. The flexible and bulky cationic substituents of **Ni-1** and **Mn-1** porphyrins preclude their interaction in the minor groove of DNA. Consequently, these porphyrins are only able to interact with long DNA polymers by electrostatic interactions with the negative charges of the phosphate groups, which may account for the previously observed binding constants on the order of $10^4 - 10^5\ M^{-1}$.[11,56] More rigid and bulky cationic substituents, such as phenyl-pyridiniumyl groups, present on **Ni-2** porphyrin prevent the interaction of this porphyrins in the minor groove of three consecutive AT base pairs sites but proved compatible with a high binding affinity for the minor groove of longer sequences consisting of six consecutive AT base pairs where **Ni-2** was clearly a better ligand than Ni-TMPyP. Since cationic porphyrins are promising ligands for quadruplex DNA, these data on the structural modifications that influence their binding to DNA should be helpful in the design of new quadruplex selective agents based on porphyrins. Indeed, a specific G-quadruplex ligand must bind to G-quadruplex DNA with a high affinity binding constant and must not show any affinity for double-stranded DNA, whose intracellular concentration is much higher.

Acknowledgment. This research was supported by French ANR (ANR-07-BLAN-0343-01) and by Région Midi-Pyrénées. Dr. Frédéric Lopez, Institut Louis Bugnard, IFR 31, Toulouse, France, is acknowledged for SPR measurements.

Supporting Information Available: Experimental protocol for the synthesis of TMPyP porphyrins, ^{13}C NMR data for *meso*-5,10,15,20-tetrakis(4-(*N*-methyl-pyridinium-2-yl)phenyl)porphyrin tetrachloride. Polyacrylamide gel electrophoresis analysis of ds19–3AT cleavage corresponding to Figure 4A. SPR experimental part and sensorgrams. This material is available free of charge via the Internet at http://pubs.acs.org.

(56) Ding, L.; Bernadou, J.; Meunier, B. *Bioconjugate Chem.* **1991**, *2*, 201–206.